Arabian Journal of Chemistry (2020) 13, 3974–3987

King Saud University

Arabian Journal of Chemistry

www.ksu.edu.sa
www.sciencedirect.com

ORIGINAL ARTICLE

Carboxymethylcellulose-coated magnesium-layered hydroxide nanocomposite for controlled release of 3-(4-methoxyphenyl)propionic acid

Norhayati Hashim [a,b,*], Nor Saleha Misuan [a], Illyas Md Isa [a,b], Suriani Abu Bakar [b,c], Suzaliza Mustafar [a], Mazidah Mamat [d], Mohd Zobir Hussein [e], Sharifah Norain Mohd Sharif [a]

[a] *Department of Chemistry, Faculty of Science and Mathematics, Universiti Pendidikan Sultan Idris, 35900 Tanjong Malim, Perak, Malaysia*
[b] *Nanotechnology Research Centre, Faculty of Science and Mathematics, Universiti Pendidikan Sultan Idris, 35900 Tanjong Malim, Perak, Malaysia*
[c] *Department of Physics, Faculty of Science and Mathematics, Universiti Pendidikan Sultan Idris, 35900 Tanjong Malim, Perak, Malaysia*
[d] *Pusat Pengajian Sains Asas, Universiti Malaysia Terengganu, 21030 Kuala Terengganu, Terengganu, Malaysia*
[e] *Institute of Advanced Technology, Universiti Putra Malaysia, 43400 Serdang, Malaysia*

Received 16 February 2019; accepted 11 April 2019
Available online 19 April 2019

KEYWORDS

Magnesium-layered hydroxide;
3-(4-Methoxyphenyl) propionic acid;
Carboxymethylcellulose;
Direct reaction method;
Controlled release

Abstract Carboxymethylcellulose (CMC) acts as a coating material for a magnesium-layered hydroxide-3-(4-methoxyphenyl)propionate (MLH-MPP) nanocomposite via spontaneous self-assembly. The resulting product is called a magnesium-layered hydroxide-3-(4-methoxyphenyl)propionate/carboxymethylcellulose (MLH-MPP/CMC) nanocomposite. The XRD pattern of the MLH-MPP/CMC nanocomposite showed that MPP was maintained in the interlayers of the MLH, thus confirming that CMC is only deposited on the surface of the MLH-MPP nanocomposite. These findings were also supported by FTIR spectra, SEM and TEM. TGA data showed that the thermal stability of the intercalated MPP was significantly enhanced compared to pure MPP and uncoated nanocomposite. The release of MPP from the interlayers of MLH-MPP/CMC nanocomposite showed slower release than did uncoated nanocomposite and followed pseudo–second-order kinetics. Since the herbicide, MPP was released from the synthesised nanocomposite

* Corresponding author at: Department of Chemistry, Faculty of Science and Mathematics, Universiti Pendidikan Sultan Idris, 35900 Tanjong Malim, Perak, Malaysia.
E-mail address: norhayati.hashim@fsmt.upsi.edu.my (N. Hashim).
Peer review under responsibility of King Saud University.

Production and hosting by Elsevier

https://doi.org/10.1016/j.arabjc.2019.04.004

in a sustained manner, thus, it has excellent potential to be used as a controlled-release herbicide formulation.

1. Introduction

The excellent intercalation of two-dimensional layered material offers a new scope for developing composite materials at the nanoscale. Intense research has targeted the family of layered material hydroxides, such as layered double hydroxide (LDH), layered metal hydroxide (LMH) and hydroxide double salts (HDS) (Liang et al., 2004). The modification of brucite by isomorphic substitution of cations resulted in the formation of LDH, while modification of brucite may result in the formation of LMH when some part of hydroxyl groups from brucite structure are substituted by water molecule. LMH is closely related to anionic clay. The general formula to described LMH is $M^{2+}(OH)_{2-x}(A^{n-})_{x/n}{\cdot}yH_2O$, where M^{2+} is the metallic cation such as Mg^{2+}, Zn^{2+}, Co^{2+} and Ni^{2+}. A is a counterion with a negative charge (Hashim et al., 2014; Hussein et al., 2012b).

One of the unique qualities of layered materials is their ability to intercalate neutral molecules or charged chemical species into their interlayers. Another specialty of layered materials is the ability to undergo ion-exchange. The utilization of ion-exchange properties and the intercalated capability of the positive layer in LMH have contributed to the removal of organic pollutants (Braterman et al., 2004). Although the explorations of LMH are not much as LDH, this material may offer more possibilities of the metal constituents and the exchangeable interlayers anion. Recent studies have reported on the intercalation of various anions into the zinc layered hydroxide and cobalt layered hydroxide (Kasai and Fujihara, 2006; Marangoni et al., 2009; Neilson et al., 2009). In some cases, the magnetic behaviour of the LMH intercalated nanocomposites were studied as well. This include the previous researches that reported on the intercalation of 8-((p-(phenylazo)phenyl)oxy)octanoate ion for the layered copper hydroxide and the intercalation of alkylsulphonate and halide ion into the layered nickel hydroxide (Fujita and Awaga, 1997; Taibi et al., 2002, 2014). Not only cobalt, nickel and copper-layered hydroxide but also zinc-layered hydroxide have been studied intensely by researchers (Lee et al., 2010; Ma et al., 2014; Reinoso et al., 2014).

Modifications involving layered nanocomposites have been performed in order to enhance their effectiveness as storage for the active agent. A new drug delivery system that incorporated 5ASA-LDH nanocomposite into the chitosan beads coated with pectin was reported in the previous study (Ribeiro et al., 2014). Another modification that have been study is the used of chitosan as a stabilizer for the layered metal sulphophenyl phosphate that are used for the transducer surface in biosensing device (De et al., 2015). A modification that focused on the surface of LDH with the purpose to provide a protective layer on the LDH surface were also reported in recent studies (Choi et al., 2010; Kura et al., 2014). This protective layer will protect this layered nanocomposite from the acid corrosion. All the modifications that have been made on the layered nanocomposite shared the same objective which is to increase the efficiency of layered materials in CRF. The selection of coating materials plays an important role in the success of a given nanocomposite formulation in the context of herbicide delivery and other applications (Kura et al., 2014). The coating process can be done by using reconstruction, ionic exchange and spontaneous self-assembly method (Li et al., 2013). Spontaneous self-assembly method is the best method since it maintains the initial size of basal spacing and the crystalline structure of nanocomposite (Dong et al., 2013).

In the past decade, LMH have been used in various contexts, including electrodes in alkaline cells, magnetism, magneto-optics, sensor and drug delivery (Barahuie et al., 2014; Delahaye et al., 2010; Liu et al., 2012; Park and Lee, 2006; Wardani et al., 2014). LMH also helps in nuclear waste treatment and the removal of nitrogen and sulphur oxides (Xue et al., 2007). Recently, there are critically numbers of environmental issues due to the contaminants, especially in agriculture sector. The contamination will decrease the quality of ground water (Bashi et al., 2013). The herbicide was lost due to runoff and lixiviation along the soil. This runoff will reduce the concentration of herbicides in the uppermost soil layer and increase in the residual activity of the herbicide, thus contaminate the underground water. In addition most of the herbicides are decompose in the soil by the effect of microorganisms and the rate of decomposition reduces as the depth increases (Jokinen et al., 2000).

LMH can be applied as a remedy for the environment due to its unique anion exchange capability. LMH is a material that acts as a reservoir for herbicides, than it has a potential to be applied for controlled release formulation (CRF) (Bashi et al., 2013; Hashim et al., 2014; Hussein et al., 2009, 2012a). When conventional agrochemicals are applied, 90% of the agrochemical will never reach their objective to produce desired biological response at the precise time and in precise quantities required by the plants (Dubey et al., 2011). CRF can maintain the effectiveness of pesticides and fertilizers in agriculture and drug in medicine (Pérez-de-Luque and Rubiales, 2009). CRF is a smart formulation that allows for the release of active agents to the target at a controlled rate and maintains its concentration in the system within an optimum limit, over a specified period of time (Scher, 1999). CRF will prolong the activity of active agents by providing continuously low amount of pesticides, amount that are sufficient for the plants and reduced the number of applications by achieving a long period of activity duration through a single application (Akelah, 1996). Therefore, CRF has been used as a solution for these problems.

Cellulose is a carbohydrate composed of a series of hydroglucose units connected by oxygen linkages. Carboxymethylcellulose (CMC) is a derivative of cellulose, which replace CH_2OH group in the glucose with a carboxymethyl group. CMC has been used as coating material in order to decrease toxicity and enhanced the stability of nanocomposite (Zhou et al., 2014). CMC has a good compatibility and encapsulation capacity, thus it has been tried in CRF for drugs and

pesticides (Li et al., 2012). In a study involving the incorporation of CMC and the LDH nanocomposite, the results showed that the intercalated CMC have a better thermal stability than pure CMC and also pH dependent swelling behaviour (Yadollahi and Namazi, 2013). In recent research, CMC has garnered increasing attention due to its unique properties, which are high viscosity, good film-forming ability, non-toxicity, biocompatibility and importantly biodegradability (Alves and Mano, 2008; Yinzhe and Shaoying, 2013). Therefore, CMC can be readily used in many areas of agro-industry.

Herein, we pursue our previous synthesised MLH-MPP nanocomposite with the modification on the surface of MLH by using CMC as a coating material. The coating process was done through spontaneous self-assembly method and the nanocomposite formed was named as MLH-MPP/CMC nanocomposite. The synthesised nanocomposite was characterised using PXRD, FTIR, TGA/DTG, SEM and TEM in order to confirm the formation of this coated nanocomposite. To the best of our knowledge, no study has examined the release of MPP from MLH-coated CMC. Three different concentrations of sodium nitrate and sodium dihydrogen phosphate solutions were used in the release and kinetic study in order to determine the release behaviour of MPP from both nanocomposites.

2. Experimental section

2.1. Materials

Herbicide, 3-(4-methoxyphenyl)propionic acid (MPP), magnesium oxide (MgO) and carboxymethylcellulose (CMC) were purchased from Acros Organics. All the chemicals were used without further purification.

2.2. Synthesis MLH-MPP/CMC nanocomposite

MLH-MPP nanocomposite with the 0.4 M of MPP was prepared by using direct reaction method as described previously (Hashim et al., 2016). MLH-MPP nanocomposite was coated with CMC based on the previous reported by Kameshima et al. (2009) and Kura et al. (2014). 0.2 g of MLH-MPP nanocomposite was added to CMC solution (0.2 g, 50 ml). Then, the mixture was stirred for 12 h at room temperature. The precipitates were separated by centrifugation and dried at 60 °C overnight in an oven.

2.3. Characterisation

Powder X-ray diffraction (XRD) patterns were recorded on a Power Diffraction Bruker AXS using Cu Kα radiation, operated at 60 kV and 30 mA. The infrared spectra of the samples were obtained with a Thermo Nicolet 6700 Fourier Transform Infrared Spectrometer. Each sample was placed in the sample holder as KBr pallets and scanned from 4000 to 400 cm^{-1}. Thermal analyses were carried out using a Perkin Elmer Pyris 1 TGA Thermo Balance at a heating rate of 20 °C per minute in the range 25–950 °C in nitrogen atmosphere. The surface morphology of the samples was observed by a field emission scanning electron microscope (FESEM) instrument, Hitachi Model SU 8020 UHR. Transmission electron microscopy (TEM) micrographs were taken using the same instrument as the surface morphology analyses.

2.4. Controlled release study

The release of MPP from the interlayers of MLH-MPP/CMC nanocomposite was conducted in several concentrations of sodium nitrate and sodium dihydrogen phosphate solutions as release media. 3 ml of sodium nitrate solution was poured into a cuvette. Then, 0.6 mg of MLH-MPP/CMC was added into the sodium nitrate solution. Next, the cuvette was covered with a lid and wrapped with parafilm. Similar step were repeated by replacing the sodium nitrate solution with the sodium dihydrogen phosphate solution. The MPP concentration in the release media was determined using Perkin Elmer UV–Vis Spectrophotometer Lambda 25 at λ_{max} = 219.0 nm.

3. Results and discussion

3.1. PXRD analysis

The XRD pattern of CMC, magnesium oxide/CMC (MCM) and MLH-MPP/CMC nanocomposite are shown in Fig. 1. CMC was represented by the broad peak that exists at approximately 20.7°, which indicates a semi-crystalline structure for CMC. The appearance of the CMC broad peak is similar with those obtained in previous study (El Sayed et al., 2015).

As shown in Fig. 1, the XRD pattern of the MLH-MPP/CMC nanocomposite represents the superposition of MCM and pure CMC. The XRD patterns of MLH-MPP/CMC nanocomposite shows an intercalation peak at the lower angle of 2θ with the basal spacing, of 17.6 Å, proved that MPP anion was maintained in the interlayers of MLH. The intercalation peak of MLH-MPP/CMC nanocomposite showed less crystallinity compared to MLH-MPP nanocomposite which due to the amorphous organic polymer that coat nanocomposite (Gangopadhyay and De, 1999; Javid et al., 2014). In comparison to previous work on the basal spacing of MLH-MPP nanocomposite, the basal spacing of MLH-MPP/CMC nanocomposite is slightly smaller (Hashim et al., 2016). The decreasing of basal spacing of MLH-MPP/CMC nanocomposite was resulted from the small change in configuration of the interlayers anion, MPP. This may be due to the decrease in MPP tilt, which presented the MPP as lying almost horizontal to the host layer. This results is in good agreement with those obtained in the previous study (Yang et al., 2007). Table 1 shows the value of basal spacing for the MLH-MPP and MLH-MPP/CMC nanocomposites. The intense peaks appeared especially for the 003 reflection at 4.64° and 4.95° for MLH-MPP and MLH-MPP/CMC nanocomposite, respectively. The 003 reflection is a typical peak for the hydrotalcite-type materials, which showed the interlayers distance of the synthesised nanocomposite, and the intensity are related with the crystallinity degree of the material (Mantilla et al., 2010).

Based on the XRD pattern of MCM, no peak can be observed at the lower angle of 2θ, which indicates the lack of any intercalation in the MCM. The result shows that there is no possibility for CMC to undergo ion exchange with the MPP herbicides, even though the presence of CMC can be seen at 20.7° in XRD pattern of MLH-MPP/CMC nanocomposite. Therefore, the addition of CMC into the MLH-MPP

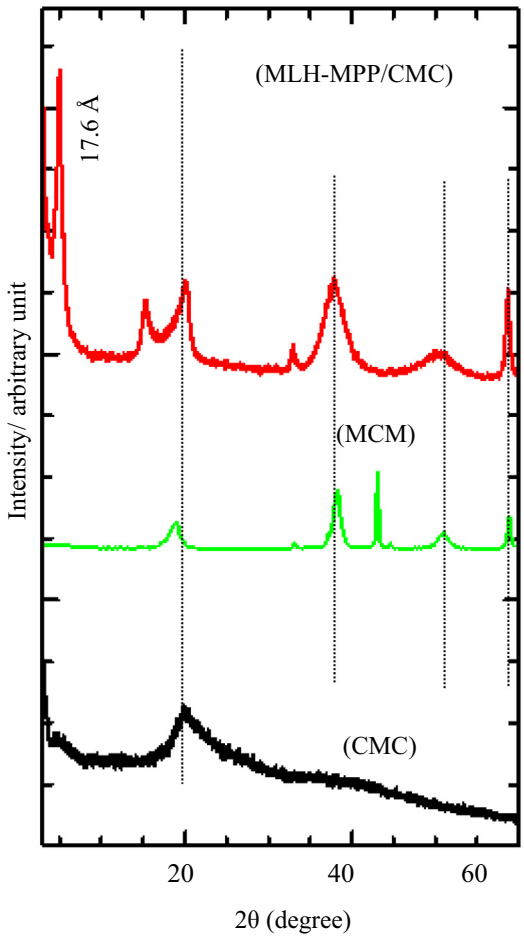

Fig. 1 PXRD patterns of MLH-MPP/CMC nanocomposite, MgO-CMC (MCM) and CMC.

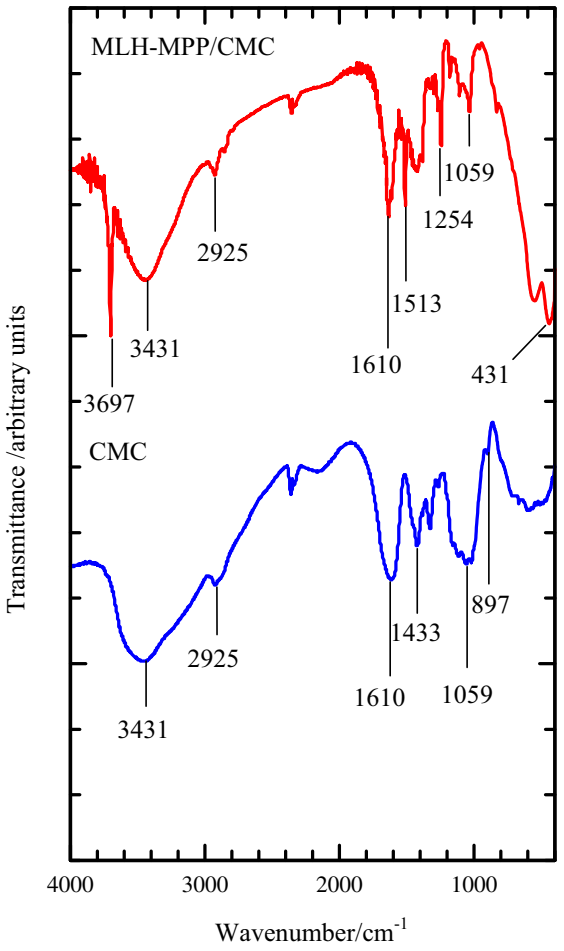

Fig. 2 The FTIR spectra of CMC and MLH-MPP/CMC nanocomposite.

nanocomposite only resulted in the adsorption of the polymer on the surface of MLH-MPP nanocomposite.

3.2. FTIR analysis

The CMC is a linear, long-chain, water-soluble, anionic polysaccharide derived from cellulose (Bono et al., 2009). Fig. 2 shows the FTIR spectra of CMC and MLH-MPP/CMC nanocomposite.

Based on the FTIR spectrum of CMC, the appeared of band at wavenumber 897 cm^{-1} associated with the β-(1,4)-glycosidic linkages between the glucose units in cellulose (Viera et al., 2007). The presence of strong band in both spectra can be observed around 1059 cm^{-1} due to C-O stretching vibration of hydroxyl groups at various positions of glucopyranose units. Previous work have reported that the presence of carboxyl groups, and its salts can be identified with the appeared of two bands at the wavenumber about 1600–1640 cm^{-1} and 1400–1450 cm^{-1} (Pescok et al., 1976). Both FTIR spectra of CMC and MLH-MPP/CMC nanocomposite demonstrate the presence of a carboxymethyl substituent at 1610 cm^{-1} and 1433 cm^{-1}. Meanwhile, the visible band at 2925 cm^{-1} is attributed to C-H stretching vibration (Biswal and Singh, 2004). The broad band around 3431 cm^{-1} is corresponding to the free O-H stretching vibration as well as inter- and intra-molecular hydrogen bonds that are presence in both CMC molecule and MLH-MPP/CMC nanocomposite.

The band at 1254 cm^{-1} in the MLH-MPP/CMC nanocomposite spectrum corresponds to the presence of asymmetrical stretching vibrations of C-O-C, while the symmetrical stretching vibrations can be seen in the range of 1200–1000 cm^{-1}. The band appearing at the wavenumber 1513 cm^{-1} indicated the presence of asymmetrical stretching vibrations of the

Table 1 Basal spacing and the peak appeared at lower angle of 2θ of MLH-MPP and MLH-MPP/CMC nanocomposite.

Nanocomposite	Basal spacing (Å)	Peaks appeared at lower angle of 2θ (deg)			Ref.
MLH-MPP	18.9	4.64	14.10	–	Hashim et al. (2016)
MLH-MPP/CMC	17.6	4.95	15.2	20.7	Present paper

carboxylate groups regards to the presence of MPP anion and the symmetrical stretching vibrations can be observed between the band 1433 cm^{-1} and 1239 cm^{-1} (Rosca et al., 2005). The bands appearing at 3697 cm^{-1} and 431 cm^{-1} for MLH-MPP/CMC nanocomposite spectrum revealed the presence of multi-coordinate hydroxyl groups of MgO and metal-oxygen bonds in the brucite-like lattice, respectively (Darder et al., 2005; Wang et al., 2011). These peaks indicated that the MLH-MPP nanocomposite was present in the coated nanocomposite. The FTIR spectra in Fig. 2 have revealed the successful coated of MLH-MPP nanocomposite with CMC.

3.3. Thermal analysis

TGA/DTG is a method used to determine the thermal stability of materials through the measure of weight change with temperature. The TGA and DTG analyses obtained for MLH-MPP nanocomposite, CMC and MLH-MPP/CMC nanocomposite are shown in Fig. 3.

The decomposition of MLH-MPP nanocomposite takes place through the dehydration, dehydroxylation of MLH and the decomposition of intercalated MPP, as similar with the previous study (Saifullah et al., 2013). The weight loss for the removal of surface and intercalated water between the ranges 47 °C to 140 °C is 8.0%. Meanwhile, the MLH began to degrade at 300 °C and the final temperature is around 400 °C, with the weight loss 23.5%. The maximum temperature and weight loss for the degradation of intercalated MPP is 475 °C and 24.5%, respectively.

The thermograms for CMC show that two stages of weight loss occurred. The first peak is observed at the 74 °C with 12.5% weight loss corresponding to the dehydration of CMC. Meanwhile, second peak is observed at 348 °C with 42.4% weight loss. The second weight loss was attributed to the degradation of side chains and the loss of carbon dioxide from CMC.

Four stages of weight loss were seen for MLH-MPP/CMC nanocomposite. The stages of weight losses of MLH-MPP/CMC nanocomposite are similar to the Dopa-LDH nanocomposite coated with Tween-80 that has been reported in previous work (Kura et al., 2014). The first stage of weight loss refers to the removal of external surface-adsorbed and interlayers water molecules, while the second stage of weight loss refers to the decomposition of CMC and partial dehydroxylation of MLH. The third and fourth stages of weight loss corresponded to further dehydroxylation of the layers and decomposition of MPP anions, respectively. The percentage weight loss for every stage in the degradation of MLH-MPP nanocomposite, CMC and MLH-MPP/CMC nanocomposite is tabulated in Table 2. The maximum temperature of the MLH-MPP nanocomposite was 475 °C which is lower than the MLH-MPP/CMC nanocomposite with the value of 797 °C. The results showed that coated nanocomposite have enhanced thermal stability compared to uncoated nanocomposite. The total weight loss of MLH-MPP nanocomposite is 56.0%, while 66.6% for MLH-MPP/CMC nanocomposite. The difference of weight loss indicated that 10.6% of CMC is successful coated on the surface of MLH-MPP/CMC nanocomposite.

3.4. Morphological analysis

Fig. 4 shows the surface morphology of commercial CMC and MLH-MPP/CMC nanocomposite analysed using FESEM. The interaction between commercial CMC and MLH-MPP nanocomposite have change the surface morphology of the commercial CMC. This result was consistence with recent study (Barkhordari et al., 2014). The CMC shows a fracture-surface image with undulant and rough structure. The morphology of MLH–MPP nanocomposite without coating material shows a flake-like structure (Hashim et al., 2016). After being coated with CMC, the flake-like structure is not clearly seen. CMC seems to provide compaction to the surface of MLH-MPP nanocomposite, thus it results the less clear of the earlier flake-like structure.

3.5. Transmission electron microscopy analysis

Fig. 5 shows a TEM image of the MLH-MPP/CMC nanocomposite. As shown in the image, the presence of a black region was due to MLH-MPP nanocomposite meanwhile, the existence of CMC is represented by the lighter shells. Based on that figure, it revealed that the MLH-MPP nanocomposite has been coated with the CMC.Fig. 6.

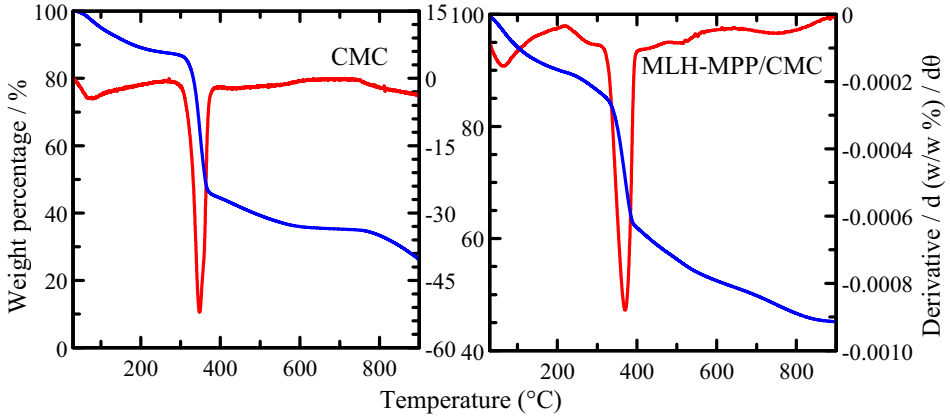

Fig. 3 TGA/DTG thermograms of CMC and MLH-MPP/CMC nanocomposite.

Table 2 TGA/DTG data on weight loss for CMC and MLH-MPP/CMC nanocomposite.

Sample	Step 1		Step 2		Step 3		Step 4		Total weight loss (%)
	Weight loss (%)	Max temp. (°C)	Weight loss (%)	Max temp. (°C)	Weight loss (%)	Max temp. (°C)	Weight loss (%)	Max temp. (°C)	
MLH-MPP	8.0	89	23.5	353	24.5	475			56.0
CMC	12.5	74	42.4	348	–	–	–	–	54.9
MLH-MPP/CMC	12.5	70	37.1	374	9.1	515	7.9	797	66.6

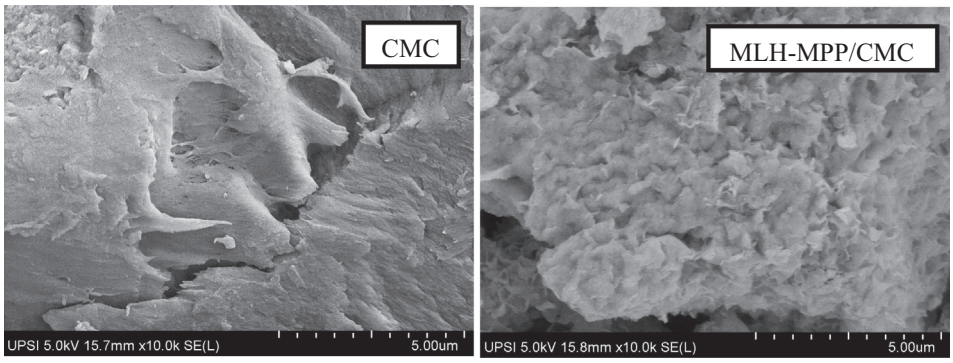

Fig. 4 The FESEM micrograph of CMC and MLH-MPP/CMC nanocomposite at 10 k magnification.

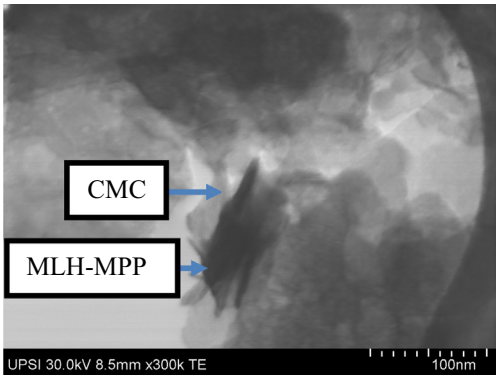

Fig. 5 TEM micrograph of MLH-MPP/CMC nanocomposite at 300 k magnification.

3.6. MPP herbicide release properties

The release of MPP from the interlayers of MLH-MPP/CMC nanocomposite was determined at $\lambda_{max} = 219.0$ nm using UV–Vis Spectrophotometer. The release study of MPP from the interlayers of the MLH-MPP/CMC nanocomposite were carried out using sodium nitrate and sodium dihydrogen phosphate solutions, with several initial concentrations: 5.0×10^{-6} M, 1.0×10^{-5} M, and 8.0×10^{-4} M. The percentage loading of MPP (%w/w) in the interlayer gallery of the MLH-MPP has been determined in the previous study, which is 42.19% (Hashim et al., 2016).

In this study, dihydrogen phosphate and nitrate were selected as the sacrificial anions in the release media, owing to the fact that these anions are numerously found in the

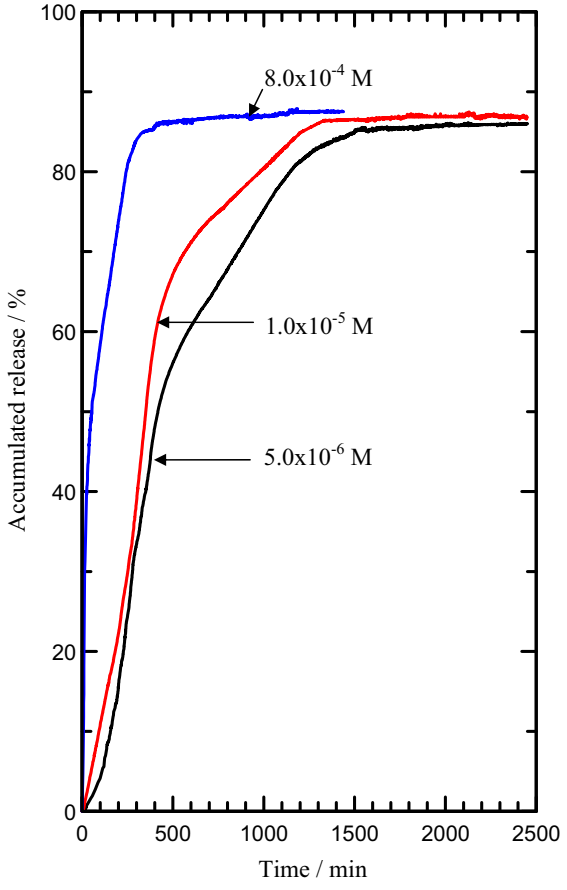

Fig. 6 . Release profile of MPP from the interlamellae of the MLH-MPP nanocomposite into solutions containing various concentrations of NaH_2PO_4.

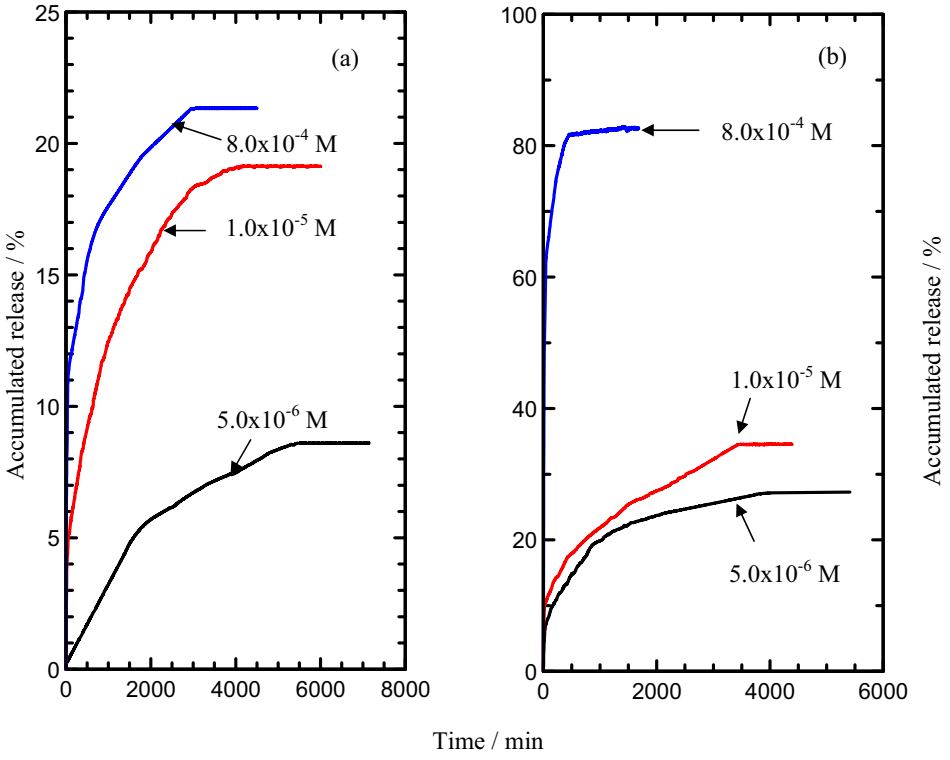

Fig. 7 Release profile of MPP from the interlamellae of the MLH-MPP/CMC nanocomposite into solutions containing various concentrations of (a) NaH_2PO_4 and (b) $NaNO_3$.

Table 3 Percentage release (%) of MPP anion from the interlayers of MLH-MPP and MLH-MPP/CMC nanocomposites into various concentrations of sodium dihydrogen phosphate solution.

Concentrations of nitrate solution (mol L^{-1})	Accumulated release (%)	
	MLH-MPP nanocomposite	MLH-MPP/CMC nanocomposite
5.0×10^{-6}	85	9
1.0×10^{-5}	87	19
8.0×10^{-4}	88	21
Ref.	Present paper	Present paper

Table 4 Percentage release (%) of MPP anion from the interlayers of MLH-MPP and MLH-MPP/CMC nanocomposites into various concentrations of nitrate solution.

Concentrations of nitrate solution (mol L^{-1})	Accumulated release (%)	
	MLH-MPP nanocomposite	MLH-MPP/CMC nanocomposite
5.0×10^{-6}	84	10
1.0×10^{-5}	85	12
8.0×10^{-4}	86	82
Ref.	Hashim et al. (2016)	Present paper

groundwater and rain water (Hashim et al., 2014). Nitrate is also classified as one of the most problematic and most common potential groundwater contaminants (Keeney and Olson, 1986). In a recent study that determine the water quality at Semenyih River, Malaysia, the result shows that the river was polluted with several chemical substances including nitrate (Al-Badaii et al., 2013). Therefore, the aqueous solutions containing nitrate and dihydrogen phosphate are the most suitable used as the release media to perform the controlled release study of MPP herbicide from the interlayers of an MLH-MPP/CMC nanocomposite.

As can be seen in Fig. 7, the release profile shows that the amounts of MPP released from various initial concentration of sodium dihydrogen phosphate solution are 85% (5.0×10^{-6} M), 87% (1.0×10^{-5} M) and 88% (8.0×10^{-4} M). Hence, indicate that the accumulated release percentage of MPP into sodium dihydrogen phosphate solution is higher than the sodium nitrate solution. In the release of MPP from the interlayers of MLH-MPP/CMC nanocomposite, the percentage release in sodium dihydrogen phosphate solution were found to be 9%, 19% and 21% at the concentration of 5.0×10^{-6} M, 1.0×10^{-5} M and 8.0×10^{-4} M, respectively (Fig. 7(a)).

Fig. 7(b) shows the release profile of MPP from the interlayers of the MLH-MPP/CMC nanocomposite into sodium nitrate. As shown in the Fig. 7(b), a rapid release of MPP from the interlayers of MLH-MPP/CMC nanocomposite can be seen around the first 30–40 min, and then followed by a sustained release. By comparing with the previous work done, the accumulated release of MPP from MLH-MPP and MLH-MPP/CMC nanocomposites were shown in Table 3

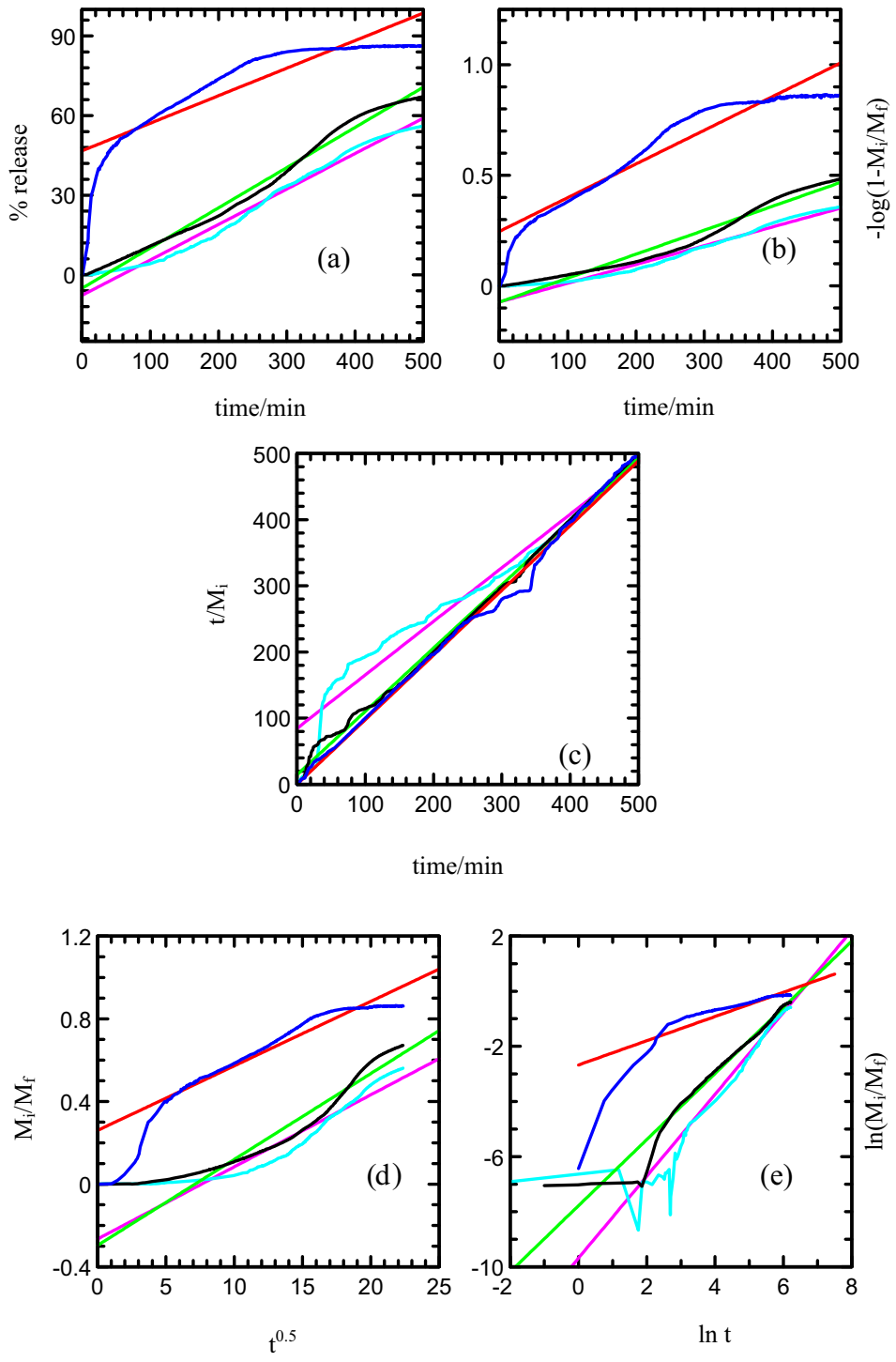

Fig. 8 Fitting of the data of MPP released from MLH-MPP nanocomposite into solution containing various concentration of NaH_2PO_4; 5.0×10^{-6} M (turquoise), 1.0×10^{-5} M (black) and 8.0×10^{-4} M (blue) to the (a) zeroth, (b) first, (c) pseudo-second order, (d) parabolic diffusion and (e) Fickian diffusion models.

(Hashim et al., 2016). The percentage accumulated release of MPP from the interlayers of MLH-MPP nanocomposite in sodium nitrate solution were 84%, 85% and 86% at the concentration of 5.0×10^{-6} M, 1.0×10^{-5} M and 8.0×10^{-4} M, respectively. Meanwhile the release of MPP from the interlayers of MLH-MPP/CMC nanocomposite in sodium nitrate solution were 10%, 12% and 82% at the concentration of 5.0×10^{-6} M, 1.0×10^{-5} M and 8.0×10^{-4} M, respectively.

As the concentration of the sodium dihydrogen phosphate and sodium nitrate solutions increases, the percentage accumulated release of MPP from the interlayers of nanocomposites also increases. This is due to the increasing of sacrificial anions

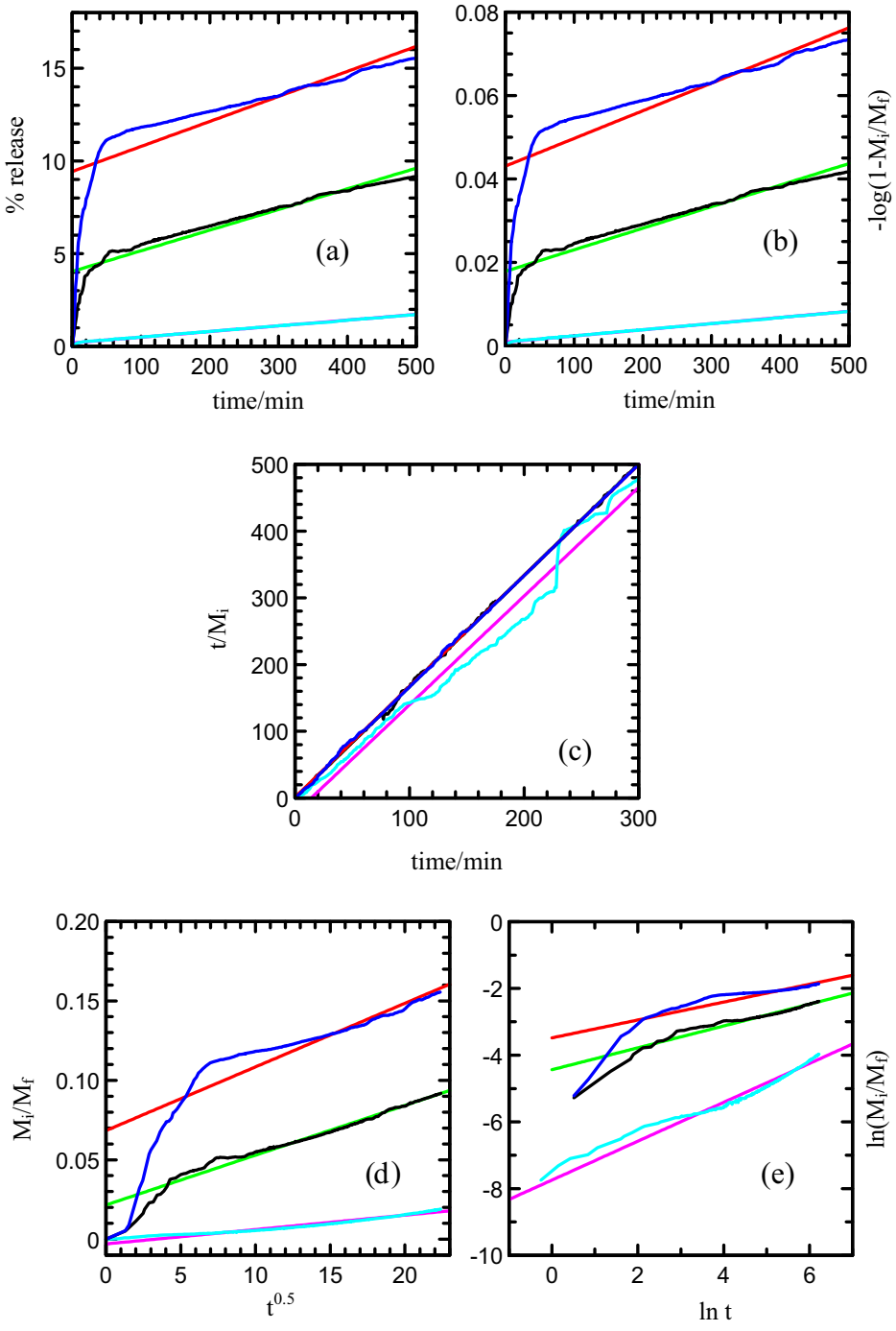

Fig. 9 Fitting of the data of MPP released from MLH-MPP/CMC nanocomposite into aqueous solution containing various concentration of NaH_2PO_4; 5.0×10^{-6} M (turquoise), 1.0×10^{-5} M (black) and 8.0×10^{-4} M (blue) to the (a) zeroth, (b) first, (c) pseudo-second order, (d) parabolic diffusion and (e) Fickian diffusion models.

along with the increasing concentration in the release solutions. The presence of these sacrificial anions will enhance the release of MPP from the interlayers of nanocomposite, thus heightening the accumulated release of MPP. These results are therefore, is in good agreement with those obtained in previous studies (Hussien et al., 2009).

The release rate of MPP from the interlayer of nanocomposite is quite fast at the first 40 min in dihydrogen phosphate solution, and the equilibrium is achieved at 1658 min (5.0×10^{-6} M), 1341 min (1.0×10^{-5} M) and 539 min (8.0×10^{-4} M). As for the release of MPP from the interlayers of MLH-MPP/CMC nanocomposite in dihydrogen phosphate solution, the equilibrium is achieved at 5612 min (5.0×10^{-6} M), 4072 min (1.0×10^{-5} M) and 3002 min (8.0×10^{-4} M). The saturated release of MPP from MLH-MPP nanocomposite in sodium nitrate solution was achieved at 530 min, 500 min and 140 min whereas, 3449 min, 3436 min and 1270 min for MLH-MPP/CMC nanocomposite along with the increased

Table 5 Correlation coefficients, rate constants and half life ($t_{1/2}$) obtained from the data of MPP release from the interlayers of MLH-MPP and MLH-MPP/CMC nanocomposite into sodium dihydrogen phosphate solution.

0–500 min								
Na_2HPO_4 (mol L^{-1})	Zeroth Order	First Order	Parabolic Diffusion	Fickian Diffusion	Pseudo-second Order			
r^2					r^2	k (x 10^{-2})s^{-1}	$t_{1/2}$ (min)	c
5.0×10^{-6}	0.977	0.959	0.874	0.933	0.954	7.77	368.29	84.4
1.0×10^{-5}	0.988	0.960	0.924	0.978	0.997	63.29	321.95	14.5
8.0×10^{-4}	0.740	0.900	0.889	0.745	0.994	6783.60	41.46	−0.14
5.0×10^{-6}	0.998	0.998	0.961	0.966	0.982	0.12	1412.68	22.90
1.0×10^{-5}	0.909	0.916	0.971	0.932	1.000	44.27	538.54	−0.06
8.0×10^{-4}	0.696	0.719	0.826	0.718	1.000	2.19	39.02	1.26

concentration. This is therefore, indicate higher release rate were observed when the MPP herbicides were released in sodium nitrate solution, compare to dihydrogen phosphate solution. The CMC coating process were also proven to greatly enhance the controlled release behaviour of the MLH-MPP nanocomposite. These results were interpreted on the basis of the ion-exchange process between the MPP and anions in the release solution.

The release rate of MPP is faster in sodium nitrate solutions than in the sodium dihydrogen phosphate solution, which is due to the differences in molecular geometry own by the dihydrogen phosphate and nitrate. Molecular geometry of nitrate is a trigonal planar geometry while the dihydrogen phosphate have a tetrahedral geometry (Bowman-James, 2005). Nitrate can be intercalated with flat-lying structure which is much easier compared to dihydrogen phosphate, thus increase the release rate of MPP herbicide. Meanwhile for tetrahedral anions, there are two possible ideal configurations that occur in the LMH interlayer, which are pyramidal configuration with its C_3 axis perpendicular to the hydroxide layer whereas C_2 axis will be perpendicular to the hydroxide layer for the second configuration (Braterman et al., 2004). Therefore, the intercalation process of dihydrogen phosphate into the interlayer of MLH needs more time compared to nitrate.

The release patterns of MPP from MLH-MPP and MLH-MPP/CMC nanocomposites are generally the same for both solutions. The initial release is faster and has slowed down afterward until equilibrium is achieved. The phenomenon occurred are similar to previous study reported by Ambrogi et al. (2001). The release of herbicide anion is controlled by the rigidity of layers and the diffusion path length. is considered as a semirigid material. The intercalated herbicide will be exchanged with the smaller species, nitrate or dihydrogen phosphate, and resulting in the decrease of basal spacing of nanocomposite. This phase transformation will initially begin on the external part of nanocomposite crystals. When the smaller and larger anions co-exist in the same crystal, there will be a formation of phase boundary. As the ion-exchange proceeds, phase boundary moves to the centre part of the crystal and the herbicides release process will become slower.

Even though the release patterns of MPP from MLH-MPP and MLH-MPP/CMC nanocomposites are generally the same for both solutions, the time needed to achieve the equilibrium release of MPP from MLH-MPP/CMC nanocomposite into the sodium dihydrogen phosphate and sodium nitrate solutions is longer than MLH-MPP nanocomposite. Moreover, the accumulated release of MPP from MLH-MPP and MLH-MPP/CMC nanocomposites into both dihydrogen phosphate and sodium nitrate solutions are quite different.

As shown in Tables 3 and 4, MLH-MPP nanocomposite coated with CMC gave a better protection to MPP herbicides than uncoated nanocomposite, since it took up to 3002 min to release 21% of MPP and 1270 min to release 82% of MPP in sodium dihydrogen phosphate and sodium nitrate solutions, respectively. This result is closely related with the increase in diffusion distance of MPP herbicide for coated nanocomposite, before release from the MLH interlayers. The increases in the diffusion distance of MPP herbicide before it is released from the MLH interlayers causing the ion-exchange process becomes slower and therefore, increases the time taken for MPP to be released. The trigonal planar geometry, nitrate is easy to be diffused and undergoes ion-exchange process with the intercalated anion, MPP herbicide. Therefore, MPP herbicide is favourable to be released in sodium nitrate solution compared to the sodium dihydrogen phosphate solution. This observation shows good agreement with the previous study that reported on the release of isoproturon and imidacloprid from alginate-bentonite-activated carbon formulation (Garrido-Herrera et al., 2006). This result demonstrates that the release of MPP from MLH-MPP/CMC nanocomposites is affected by the diffusion distance of MPP and the geometry of the anions provided by the release solution. The controlled release study of the MLH-MPP/CMC nanocomposite conducted is therefore, proven that the CMC is an effective inorganic matrix for the herbicides storage, and the release of MPP herbicide can be extended, and it is safe for the environment.

3.7. Kinetic study

The kinetic study was done in order to clarify the mechanism by which MPP is released from the MLH-MPP/CMC nanocomposite. The data obtained from the release study of coated nanocomposite were furthered with the kinetic study by using commonly five different kinetic models; which are zeroth order (Lobo and Costa, 2001), first order (Abdul Latip et al., 2013), pseudo-second order (Kura et al., 2014), parabolic diffusion (Hussein et al., 2011) and Fickian diffusion kinetic models (Hashim et al., 2014). The equations for each kinetic models are required as below:

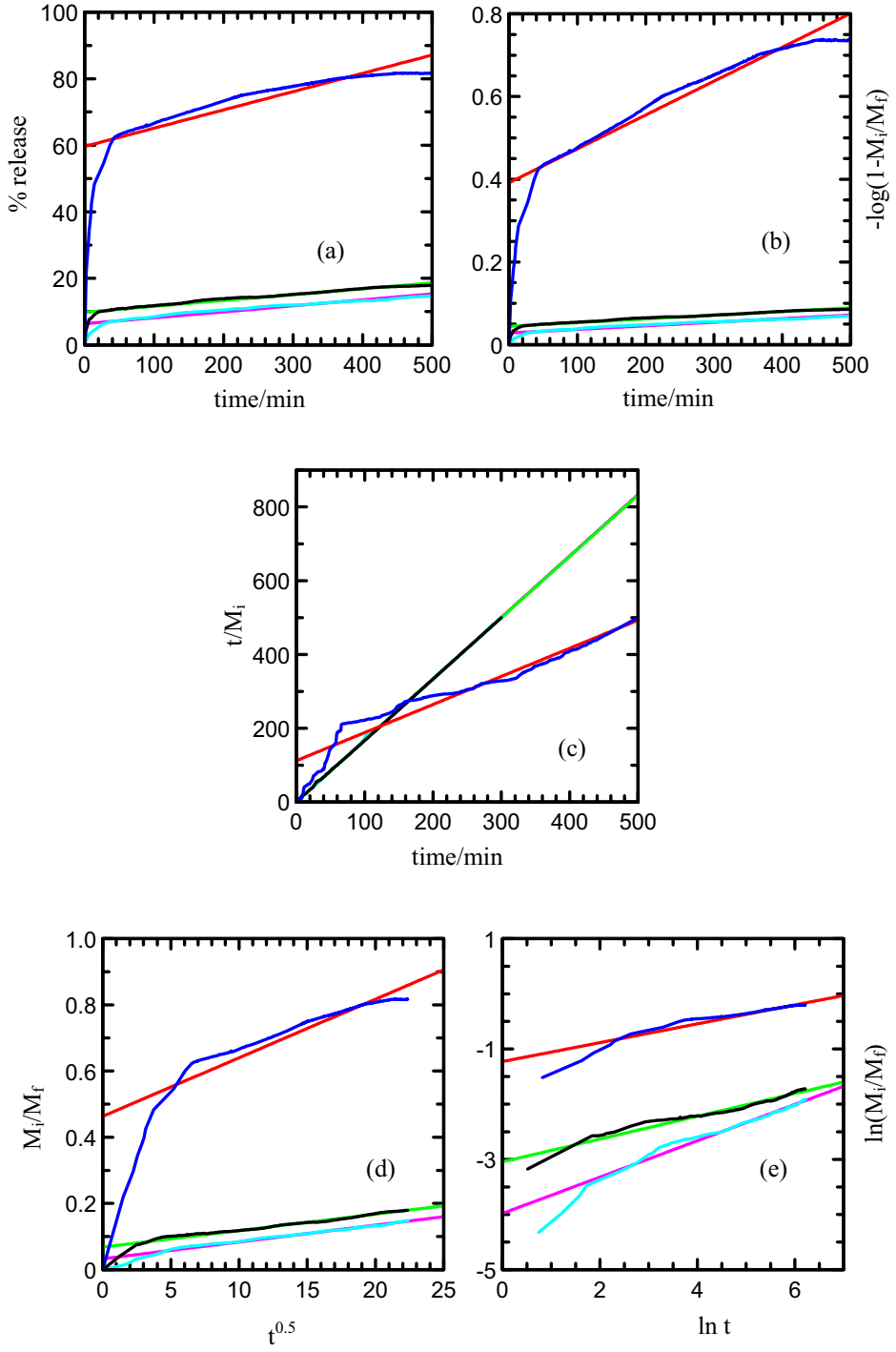

Fig. 10 Fitting of the data of MPP released from MLH-MPP/CMC nanocomposite for into aqueous solution containing various concentration of nitrate; 5.0×10^{-6} M (turqoise), 1.0×10^{-5} M (black) and 8.0×10^{-4} M (blue) to the (a) zeroth, (b) first, (c) pseudo-second order, (d) parabolic diffusion and (e) Fickian diffusion models.

Zeroth order model:	$x = t + c$
First order model:	$-\log(1-M_i/M_f) = t + c$
Pseudo-second order model:	$t/M_i = 1/(M_f^2) + t/M_f$
Parabolic diffusion model:	$M_i/M_f = kt^{0.5} + c$
Fickian diffusion model:	$M_i/M_f = kt^n$

where M_i and M_f are referred to the initial and final concentration of MPP herbicides, respectively, while n is an empirical parameter describing the release mechanism and c is a constant. The value of x corresponds to the percentage release of MPP herbicide at time t. The parameter correlation coeffi-

Table 6 Correlation coefficients, rate constants and half life ($t_{1/2}$) obtained from the data of MPP release from the interlayers of MLH-MPP/CMC nanocomposite into sodium nitrate solutions.

0–500 min								
$NaNO_3$ (mol L^{-1})	Zeroth order	First order	Parabolic diffusion	Fickian diffusion	Pseudo-second order			
	r^2				r^2	k ($\times 10^{-2}$)s^{-1}	$t_{1/2}$ (min)	c
5.0×10^{-6}	0.908	0.919	0.980	0.971	1.000	367.44	431.00	0.76
1.0×10^{-5}	0.916	0.929	0.963	0.958	1.000	283.79	396.96	0.97
8.0×10^{-4}	0.630	0.853	0.802	0.917	0.930	0.52	7.38	112.00

cients, r^2, rate constant, k and $t_{1/2}$ values are calculated based on the listed equations.

Kinetic study for the release of MPP from the MLH-MPP nanocomposite interlayer is performed by using the qualitative analysis. Figs. 8 and 9 show the fitting of the release data between 0 and 500 min for MPP release from the interlayers of MLH-MPP and MLH-MPP/CMC nanocomposite into sodium dihydrogen phosphate solution, respectively. The best fitted graph can be obtained when the resultant r^2 values are closest to 1. As shown in Table 5 zeroth order is seemed to be unsuitable for describing the mechanism due to its low r^2 value. The first order, parabolic diffusion and Fickian diffusion models also resulted in poor linearity. The fitting of the release data for MLH-MPP and MLH-MPP/CMC nanocomposites in the sodium dihydrogen phosphate solution is best achieved with the pseudo-second order model as is evident by the high r^2 values. Pseudo-second order has elucidated that the release of herbicide from the inorganic MLH interlayer is involved in the dissolution of nanocomposite as well as ion exchange between the intercalated anions in the MLH interlayer and nitrate anions in the aqueous solution. The similar results has been reported by Hashim et al. (2014) for the release of cloprop from cloprop-LDH nanocomposite into phosphate solution.

Fig. 10 shows the fitting for MPP release data from MLH-MPP/CMC nanocomposite into the sodium nitrate solution system between 0 and 500 min. Based on the result, the release data shows a good fitting with pseudo-second order as evident by a maximum r^2 values of 1 compared to zeroth, first, parabolic diffusion and Fickian diffusion model (Table 6). Thus, it confirms that the release of MPP from the interlayers of MLH-MPP/CMC nanocomposite into sodium nitrate solution involved the slow dissolution of MLH-MPP/CMC nanocomposite as well as ion exchange between the MPP in the interlayers of MLH with the nitrate anion present in the release solution.

Based on Tables 5 and 6, half life ($t_{1/2}$) for the release of MPP decreased as the concentration of release solution increases. These results showed that the release of MPP into the solution was found to be faster as the higher capacity anions intercalated into the interlayers of MLH through ion exchange process. The same pattern of $t_{1/2}$ value can be observed for the release dichlorprop from Zn/Al-dichlorprop synthesised using direct co-precipitation (DPPADI) nanocomposite and Zn/Al-dichlorprop synthesised using anion exchange process (DPPAEX) nanocomposite (Hussein et al., 2011a, 2011b).

4. Conclusion

In summary, CMC was successfully coated on the external surface of an MLH-MPP nanocomposite. The XRD patterns for coated nanocomposites show that the coating materials, CMC only resulted in adsorption of the polymer on the surface of the MLH-MPP nanocomposite. FTIR spectroscopy has supported the presence of CMC on the MLH-MPP nanocomposite. The thermal stability of MPP in the interlayers of MLH-MPP/CMC nanocomposite was remarkably enhanced. Based on this result, coated nanocomposite shows the ability to prolong the release of MPP from the interlayers of MLH, thus proving that the CMC-coated MLH-MPP nanocomposite could enhance the controlled release behaviour of this particular nanocomposite. The release of MPP from the interlayers of synthesised coated nanocomposite was governed by a pseudo–second-order model, as evidenced by high r^2 values. Therefore, it can be concluded that MLH nanocomposite coated with CMC is an excellent inorganic matrix that could improve the release of MPP in the agricultural sector.

Acknowledgements

This work was supported by the FRGS Grant: 2019-0002-102-02. Thank UPSI for all affords and support in this research.

References

Abdul Latip, A.F., Hussein, M.Z., Stanslas, J., Wong, C.C., Adnan, R., Latip, A.F.A., Hussein, M.Z., Stanslas, J., Wong, C.C., Adnan, R., Abdul Latip, A.F., Hussein, M.Z., Stanslas, J., Wong, C.C., Adnan, R., Latip, A.F.A., Hussein, M.Z., Stanslas, J., Wong, C.C., Adnan, R., 2013. Release behavior and toxicity profiles towards A549 cell lines of ciprofloxacin from its layered zinc hydroxide intercalation compound. Chem. Cent. J. 7, 1–11.

Akelah, A., 1996. Novel utilizations of conventional agrochemicals by controlled release formulations. Mater. Sci. Eng. C 4, 83–98.

Al-Badaii, F., Shuhaimi-Othman, M., Gasim, M.B., 2013. Water quality assessment of the semenyih river, selangor, malaysia. J. Chem. 2013, 1–10.

Alves, N.M., Mano, J.F., 2008. Chitosan derivatives obtained by chemical modifications for biomedical and environmental applications. Int. J. Biol. Macromol. 43, 401–414.

Ambrogi, V., Fardella, G., Grandolini, G., Perioli, L., 2001. Intercalation compounds of hydrotalcite-like anionic clays with antiinflammatory agents — I. Intercalation and in vitro release of ibuprofen. Int. J. Pharmaceutics 220, 23–32.

Barahuie, F., Hussein, M.Z., Fakurazi, S., Zainal, Z., 2014. Development of drug delivery systems based on layered hydroxides for

nanomedicine. Int. J. Mol. Sci. https://doi.org/10.3390/ijms15057750.
Barkhordari, S., Yadollahi, M., Namazi, H., 2014. pH sensitive nanocomposite hydrogel beads based on carboxymethyl cellulose/layered double hydroxide as drug delivery systems. J. Polym. Res. 21, 454.
Bashi, A.M., Hussein, M.Z., Zainal, Z., Tichit, D., 2013. Synthesis and controlled release properties of 2,4-dichlorophenoxy acetate-zinc layered hydroxide nanohybrid. J. Solid State Chem. 203, 19–24.
Biswal, D.R., Singh, R.P., 2004. Characterisation of carboxymethyl cellulose and polyacrylamide graft copolymer. Carbohydr. Polym. 57, 379–387.
Bono, A., Ying, P.H., Yan, F.Y., Muei, C.L., Sarbatly, R., Krishnaiah, D., 2009. Synthesis and characterization of carboxymethyl cellulose from palm kernel cake. Adv. Nat. Appl. Sci. 3, 5–11.
Bowman-James, K., 2005. Alfred Werner revisited: the coordination chemistry of anions. Acc. Chem. Res. 38, 671–678.
Braterman, P.S., Xu, Z.P., Yarberry, F., 2004. Layered Double Hydroxide. In: Auerbach, S.M., Carrado, K.A., Dutta, P.K. (Eds.), Handbook of Layered Materials. Marcel Dekker Inc, New York, pp. 373–449.
Choi, G., Lee, J.-H., Oh, Y.-J., Choy, Y Bin, Park, M.C., Chang, H. C., Choy, J.-H., 2010. Inorganic-polymer nanohybrid carrier for delivery of a poor-soluble drug, ursodeoxycholic acid. Int. J. Pharm. 402, 117–122.
Darder, M., Blanco-Lopez, M., Aranda, P., Leroux, F., Ruiz-hitzky, E., 2005. Bio-nanocomposites based on layered double hydroxides. Chem. Mater. 17, 1969–1977.
De, S., Mohanty, S., Nayak, S.K., 2015. Structure-property relationship of layered metal oxide phosphonate/chitosan nanohybrids for transducer in biosensing device. J. Mater. Eng. Perform. 24, 114–127.
Delahaye, É., Eyele-Mezui, S., Diop, M., Leuvrey, C., Rabu, P., Rogez, G., 2010. Rational synthesis of chiral layered magnets by functionalization of metal simple hydroxides with chiral and non-chiral Ni(II) Schiff base complexes. Dalt. Trans. 39, 10577–10580.
Dong, L., Gou, G., Jiao, L., 2013. Characterization of a dextran–coated layered double hydroxide acetylsalicylic acid delivery system and its pharmacokinetics in rabbit. Acta Pharm. Sin. B 3, 400–407.
Dubey, S., Jhelum, V., Patanjali, P.K., 2011. Controlled release agrochemicals formulations: a review. J. Sci. Ind. Res. (India) 70, 105–112.
El Sayed, A.M., El-Gamal, S., Morsi, W.M., Mohammed, G., 2015. Effect of PVA and copper oxide nanoparticles on the structural, optical, and electrical properties of carboxymethyl cellulose films. J. Mater. Sci. 50, 4717–4728.
Fujita, W., Awaga, K., 1997. Reversible structural transformation and drastic magnetic change in a copper hydroxides intercalation compound. J. Am. Chem. Soc. 7863, 4563–4564.
Gangopadhyay, R., De, A., 1999. Polypyrrole-ferric oxide conducting nanocomposites I. Synthesis and characterization. Eur. Polym. J. 35, 1985–1992.
Garrido-Herrera, F.J., Gonzalez-Pradas, E., Fernandez-Peres, M., 2006. Controlled release of isoproturon, imidacloprid, and cyromazine from alginate−bentonite-activated carbon formulations. J. Agric. Food Chem. 54, 10053–10060.
Hashim, N., Hussein, M.Z., Isa, I., Kamari, A., Mohamed, A., Jaafar, A.M., Taha, H., 2014. Synthesis and controlled release of cloprop herbicides from cloprop-layered double hydroxide and cloprop-zinc-layered hydroxide nanocomposites. Open J. Inorg. Chem. 4, 1–9.
Hashim, N., Misuan, N.S., Md Isa, I., Kamari, A., Mohamed, A., Bakar, S.A., Hussein, M.Z., 2016. Development of a novel nanocomposite consisting of 3-(4-methoxyphenyl)propionic acid and magnesium layered hydroxide for controlled-release formulation. J. Exp. Nanosci. 11, 776–797. https://doi.org/10.1080/17458080.2016.1171916.
Hussein, M.Z. bin, Ghotbi, M.Y., Yahaya, A.H., Abd Rahman, M.Z., 2009. Synthesis and characterization of (zinc-layered-gallate) nanohybrid using structural memory effect. Mater. Chem. Phys. 113, 491–496.
Hussein, M.Z., Al Ali, S.H., Zainal, Z., Hakim, M.N., 2011a. Development of antiproliferative nanohybrid compound with controlled release property using ellagic acid as the active agent. Int. J. Nanomedicine 6, 1373–1383.
Hussein, M.Z., Hashim, N., Yahaya, A., Zainal, Z., 2011b. Synthesis of dichlorprop-Zn/Al-hydrotalcite nanohybrid and its controlled release property. Sains Malaysiana 40, 887–896.
Hussein, M.Z., Nazarudin, N.F., Sarijo, S.H., Yarmo, M.A., 2012a. Synthesis of a layered organic-inorganic nanohybrid of 4-chlorophenoxyacetate-zinc-layered hydroxide with sustained release properties. J. Nanomater. 2012, 1–10.
Hussein, M.Z., Rahman, N.S.S.A., Sarijo, S.H., Zainal, Z., 2012b. Herbicide-intercalated zinc layered hydroxide nanohybrid for a dual-guest controlled release formulation. Int. J. Mol. Sci. 13, 7328–7342.
Hussien, M.Z., Ghotbi, M.Y., Yahaya, A.H., Rahman, M.Z.A., bin Hussein, M.Z., Ghotbi, M.Y., Yahaya, A.H., Abd Rahman, M.Z., 2009. The effect of polymers onto the size of zinc layered hydroxide salt and its calcined product. Solid State Sci. 11, 368–375.
Javid, A., Ahmadian, S., Saboury, A.A., Kalantar, S.M., Rezaei-Zarchi, S., 2014. Novel biodegradable heparin-coated nanocomposite system for targeted drug delivery. RSC Adv. 4, 13719–13728.
Jokinen, K., Hautala, J., Eronen, L., 2000. Effect of herbicides. 6083876.
Kameshima, Y., Sasaki, H., Isobe, T., Nakajima, A., Okada, K., 2009. Synthesis of composites of sodium oleate/Mg-Al-ascorbic acid-layered double hydroxides for drug delivery applications. Int. J. Pharm. 381, 34–39.
Kasai, A., Fujihara, S., 2006. Layered single-metal hydroxide/ethylene glycol as a new class of hybrid material. Inorg. Chem. 45, 415–418. https://doi.org/10.1021/ic051528d.
Keeney, D., Olson, R.A., 1986. Sources of nitrate to ground water. Crit. Rev. Environ. Sci. Technol. 16, 257–304.
Kura, A.U., Samer, H.H.A.A., Hussein, M.Z., Fakurazi, S., Al Ali, S. H.H., Hussein, M.Z., Fakurazi, S., 2014. Preparation of Tween 80-Zn/Al-levodopa-layered double hydroxides nanocomposite for drug delivery system. Sci. World J. https://doi.org/10.1155/2014/104246.
Lee, J.W., Choi, W.C., Kim, J.D., 2010. Size-controlled layered zinc hydroxide intercalated with dodecyl sulfate: effect of alcohol type on dodecyl sulfate template. CrystEngComm 12, 3249–3254.
Li, J., Yao, J., Li, Y., Shao, Y., 2012. Controlled release and retarded leaching of pesticides by encapsulating in carboxymethyl chitosan/bentonite composite gel. J. Environ. Sci. Heal. 47, 795–803.
Li, P., Lv, F., Xu, Z., Qi, G., Zhang, Y., 2013. Functions of surfactants in the one-step synthesis of surfactant-intercalated LDHs. J. Mater. Sci. 48, 5437–5446.
Liang, C., Shimizu, Y., Masuda, M., Sasaki, T., Koshizaki, N., 2004. Preparation of layered zinc hydroxide/surfactant nanocomposite by pulsed-laser ablation in a liquid medium. Chem. Mater. 16, 963–965.
Liu, X., Ma, R., Bando, Y., Sasaki, T., 2012. A general strategy to layered transition-metal hydroxide nanocones: tuning the composition for high electrochemical performance. Adv. Mater. 24, 2148–2153.
Lobo, M.S., Costa, P., 2001. Modeling and comparison of dissolution profiles. Eur. J. Pharm. Sci. 13, 123–133.
Ma, W., Ma, R., Liang, J., Wang, C., Liu, X., Zhou, K., Sasaki, T., 2014. Layered zinc hydroxide nanocones: synthesis, facile morphological and structural modification, and properties. Nanoscale 6, 13870–13875.
Mantilla, A., Tzompantzi, F., Fernández, J.L.L., Díaz Góngora, J.A.I. A.I., Mendoza, G., Gómez, R., 2010. Photodegradation of 2,4-

dichlorophenoxyacetic acid using ZnAlFe layered double hydroxides as photocatalysts. Catal. Today 148, 119–123.
Marangoni, R., Ramos, L.P., Wypych, F., 2009. New multifunctional materials obtained by the intercalation of anionic dyes into layered zinc hydroxide nitrate followed by dispersion into poly(vinyl alcohol) (PVA). J. Colloid Interface Sci. 330, 303–309.
Neilson, J.R., Schwenzer, B., Seshadri, R., Morse, D.E., 2009. Kinetic control of intralayer cobalt coordination in layered hydroxides: CO1-05xoctCox tet(OH)2(CI)x(H2O)n. Inorg. Chem. 48, 11017–11023.
Park, S.-H., Lee, C.E., 2006. Synthesis and characterization and magnetic properties of a novel disulfonate-pillared copper hydroxide Cu2(OH)3(DS4)1/2, DS4 = 1,4-Butanedisulfonate. Bull. Korean Chem. Soc. 27, 1587–1592.
Pérez-de-Luque, A., Rubiales, D., 2009. Nanotechnology for parasitic plant control. Pest Manag. Sci. 65, 540–545.
Pescok, R., Shields, L.D., Caims, T., McWilliam, I.G., 1976. Modern Methods of Chemical Analysis. Wiley, New York.
Reinoso, D.M., Damiani, D.E., Tonetto, G.M., 2014. Synthesis of biodiesel from soybean oil using zinc layered hydroxide salts as heterogeneous catalysts. Catal. Sci. Technol. 4, 1803.
Ribeiro, L.N.M., Alcântara, A.C.S., Darder, M., Aranda, P., Araújo-Moreira, F.M., Ruiz-Hitzky, E., 2014. Pectin-coated chitosan-LDH bionanocomposite beads as potential systems for colon-targeted drug delivery. Int. J. Pharm. 463, 1–9.
Rosca, C., Popa, M.I., Lisa, G., Chitanu, G.C., 2005. Interaction of chitosan with natural or synthetic anionic polyelectrolytes. 1. The chitosan–carboxymethylcellulose complex. Carbohydr. Polym. 62, 35–41.
Saifullah, B., Hussein, M.Z., Hussein-Al-Ali, S.H., Arulselvan, P., Fakurazi, S., 2013. Sustained release formulation of an anti-tuberculosis drug based on para-amino salicylic acid-zinc layered hydroxide nanocomposite. Chem. Cent. J. 7, 72.
Scher, H.B., 1999. Controlled-release Delivery System for Pesticides. Marcel Dekker Inc, New York.
Taibi, M., Ammar, S., Jouini, N., Fiévet, F., Molinié, P., Drillon, M., 2002. Layered nickel hydroxide salts: synthesis, characterization and magnetic behaviour in relation to the basal spacing. J. Mater. Chem. 12, 3238–3244. https://doi.org/10.1039/b204087e.
Taibi, M., Jouini, N., Rabu, P., Ammar, S., Fiévet, F., 2014. Lamellar nickel hydroxy-halides: anionic exchange synthesis, structural characterization and magnetic behavior. J. Mater. Chem. C 2, 4449.
Viera, R.G.P., Filho, G.R., de Assunção, R.M.N., Meireles, C.D.S., Vieira, J.G., de Oliveira, G.S., 2007. Synthesis and characterization of methylcellulose from sugar cane bagasse cellulose. Carbohydr. Polym. 67, 182–189.
Wang, D.-Y., Leuteritz, A., Kutlu, B., Der Landwehr, M.A., Jehnichen, D., Wagenknecht, U., Heinrich, G., 2011. Preparation and investigation of the combustion behavior of polypropylene/organomodified MgAl-LDH micro-nanocomposite. J. Alloys Compd. 509, 3497–3501.
Wardani, N.I., Isa, I.M., Hashim, N., Ghani, S.A., 2014. Zinc layered hydroxide-2(3-chlorophenoxy)propionate modified multi-walled carbon nanotubes paste electrode for the determination of nano-molar levels copper(II). Sensors Actuators, B Chem. 198, 243–248.
Xue, L., Zhang, C., He, H., Teraoka, Y., 2007. Catalytic decomposition of N_2O over CeO_2 promoted Co_3O_4 spinel catalyst. Appl. Catal. B Environ. 75, 167–174.
Yadollahi, M., Namazi, H., 2013. Synthesis and characterization of carboxymethyl cellulose/layered double hydroxide nanocomposites. J. Nanoparticle Res. 15, 1563–1572.
Yang, J.H., Han, Y.S., Park, M., Park, T., Hwang, S.J., Choy, J.H., 2007. New inorganic-based drug delivery system of indole-3-acetic acid-layered metal hydroxide nanohybrids with controlled release rate. Chem. Mater. 19, 2679–2685.
Yinzhe, R., Shaoying, Z., 2013. Effect of carboxymethyl cellulose and alginate coating combined with brewer yeast on postharvest grape preservation. Int. Sch. Res. Not. Agron. 2013, 1–7.
Zhou, L., Thanh, T Le, Gong, J., Kim, J.-H., Kim, E.-J., Chang, Y.-S., 2014. Carboxymethyl cellulose coating decreases toxicity and oxidizing capacity of nanoscale zerovalent iron. Chemosphere 104, 155–161.